

Gap Corrected Thin Film Permittivity and Permeability Measurement with a Broadband Coaxial Line Technique

Yunqi Wang, Ian Hooper, Eleanor Edwards, and Patrick S. Grant

Abstract—A technique for measuring the high frequency broadband complex permittivity and permeability of thin films from 50 MHz up to 18 GHz without the need for a reference sample for calibration is presented. A thin film for measurement is wound into a torus and inserted into a coaxial line. As a consequence, this method is suitable for measuring flexible self-supported films and coatings fabricated on flexible substrates. With the torus axis of symmetry along the coaxial direction, the electromagnetic properties of the wound torus can be deduced from the perturbed reflection and transmission coefficients of an incident wave. However, when permittivity and permeability are then obtained, there is a contribution from the effect of air gaps that cannot be avoided between layers of the wound film, which results in an underestimation of the measured permittivity and permeability. An analytical air gap correction model has been developed to account for this air gap effect that is then validated by experiments and shown also to be consistent with finite element simulations. The relative effects of film thickness and air gap on a range of measured permittivity and permeability have been also elucidated.

Index Terms—Broadband electromagnetic measurements, gap correction, permittivity, permeability, thin film characterization.

I. INTRODUCTION

THIN films with tailored permittivity and permeability properties are used in microwave communication devices [1], [2] for applications such as electromagnetic interference shielding [3], [4], electromagnetic compatibility [5], field sensors [6], and magnetic recording [7], [8]. Consequently, convenient techniques for broadband electromagnetic characterization of these films in the microwave domain are required. However, broadband measurements on films above 1 GHz can sometimes be relatively restrictive [9], [10]. Resonant cavities whose resonance frequency and quality factor Q are changed by introduction of a thin film sample, and from which the permittivity or permeability tensor can be derived, are straightforward but are limited to discrete frequencies [11]. An open-ended coaxial probe method [12] has been developed for measurements over a frequency band between 200 MHz to 20 GHz, in which the fields at the probe end fringe into the

material, becoming modified as they come into contact with the material under test. However, this method is only suitable for measuring the permittivity of the material, and a sample with a significant thickness (i.e. $h \geq 2b$, where h is the material thickness, $2b$ is the diameter of the outer conductor of the coaxial probe) is required because the wave scattering from the probe could penetrate a thin sample and impinge on other media [13]. As such, the open-ended coaxial probe method is normally not appropriate for thin film characterization. In the standard waveguide technique, the sample under test is inserted into a segment of waveguide, and both the permittivity and the permeability of the sample are derived from the measured reflection and transmission coefficients. However, when the thickness of the sample is much less than the wavelength the uncertainties in the extracted properties become large [14], making it unsuitable for thin film measurements. Methods that make use of transmissive planar circuits such as coplanar waveguides and micro-stripline techniques have been introduced for broadband thin film measurements. The film under test is measured as part of the transmission line and hence the measured result is a function of both the film and metallic conductor that make up the transmission line [15], [16]. Therefore the method used to separate the properties of the film from those of the metallic conductor becomes crucial for accurate extraction of the permittivity and permeability of the film. It has been shown in coplanar waveguide measurements (45 MHz to 40 GHz), that a calibration comparison method [17], in which two identical sets of coplanar waveguides with and without the material under test, is needed to separate the properties of the coplanar waveguide conductor from those of the film. Similarly, for a shorted micro-stripline perturbation method (100 MHz to 5 GHz), a reference sample that is similar to the sample under study in both size and response is needed for accurate measurements [18–21] and significant errors may be introduced [22].

The coaxial transmission line technique is a convenient approach that provides both permittivity and permeability measurement up to 18 GHz with no need for a reference sample. It is based on the measurement of the complex reflection and

Y. Wang and P. S. Grant are with the Department of Materials, University of Oxford, Parks Road, Oxford, OX1 3PH UK (e-mail: yunqi.wang@materials.ox.ac.uk; patrick.grant@materials.ox.ac.uk).

I. Hooper is with the Department of Physics and Astronomy, University of Exeter, Stocker Road, Exeter, EX4 4QL UK (e-mail: i.r.hooper@exeter.ac.uk).

E. Edwards is with the Department of Engineering Science, University of Oxford, Parks Road, Oxford, OX1 3PJ UK (e-mail: eleanor.edwards@eng.ox.ac.uk).

transmission amplitude coefficients of a coaxial line loaded with material that are recorded by a vector network analyser (VNA). From the changes in the coaxial line reflection and transmission coefficients upon material loading, the relative complex permittivity ($\epsilon = \epsilon' - i\epsilon''$) and permeability ($\mu = \mu' - i\mu''$) can be deduced by solving the Nicholson, Ross and Weir (NRW) equations [23], [24]. Measurement of the permeability of a thin film has been demonstrated in the case of one layer of film covering the inner conductor of a coaxial line or the outer surface of a dielectric torus [25], but significant errors when films of relatively small permittivity and permeability, which provide only small changes in the reflected and transmitted signal, can arise. Instead, the films can be wound onto the torus, generating many revolutions of winding and many concentric layers [26]. However, the films must be tightly wound with no air gaps, but in practice the elimination of air gaps is very difficult to achieve so that the deduced permittivity and permeability of the thin film may be underestimated by an unknown amount. In this paper, an equivalent circuit model for gap correction of the coaxial line thin film measurement technique is developed. This analytical approach is then validated by comparison with experimental results, and by comparing reflection and transmission data to that calculated using a simple finite element based model solved using Comsol Multiphysics software. Finally, the relative impact of the air gap and other parameters on the permittivity and permeability are discussed.

II. EXPERIMENTAL

A coaxial airline terminated with standard APC-7 connectors was used to characterize the thin film samples. This had outer conductor diameter of 7 mm and inner of 3 mm and was fabricated following the design of Lederer [27], supporting a transverse electromagnetic (TEM) waveguide mode up to 18 GHz. The coaxial line was designed and fabricated with a characteristic impedance of 50 Ω . The coaxial cell was connected to a calibrated VNA (Anritsu MS4644A) that quantified the scattering parameters of the segment of coaxial line filled with the material under test, as shown in Fig. 1. For demonstration, a Polytetrafluoroethylene (PTFE) thin film (536-4006 RS Components Ltd) of 76 μm thickness was finger-tight wound onto an inner ring of 3 mm diameter, with sufficient revolution to give a final external diameter of 7 mm, which was then inserted snugly into the coaxial cell.

Using the standard approach of NRW based on transmitted and reflected coefficients, Fig. 2(a) shows the apparent complex permittivity and permeability of the PTFE film as a function of frequency in the range 500 MHz to 10 GHz. Although there was no observable air gap in the wound film in the cell by eye, as shown in the inset of Fig. 2(a), the air fraction f_{air} of the sample was calculated to be around 12 vol. % according to the known length of the film used and the precisely known volume of the coaxial cell $\left(f_{\text{air}} = 1 - \frac{V_{\text{film}}}{V_{\text{cell}}} = 1 - \frac{l_{\text{film}} t_{\text{film}} w_{\text{film}}}{V_{\text{cell}}}\right)$, where V_{film} and V_{cell} are the volume of film and sample cell, respectively; l_{film} , t_{film} and w_{film} are the film length, thickness (76 μm), width (7

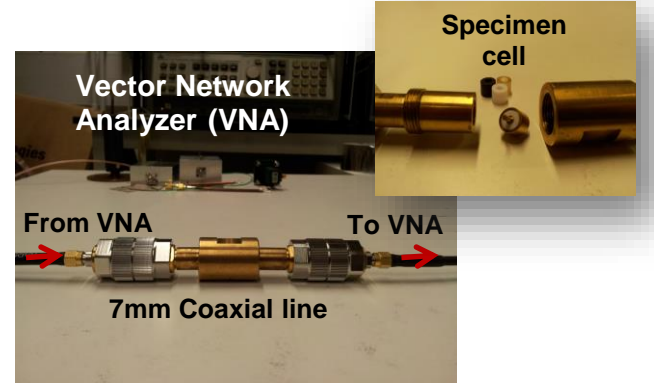


Fig. 1 Coaxial line measurement setup with ring-shaped sample under test inserted in between inner and outer conductor of the co-axial line.

mm), respectively). The measured real permittivity of the PTFE film with no air gap adjustment sample was 1.78 over the range, compared with a data sheet value of close to 2 over this frequency range.

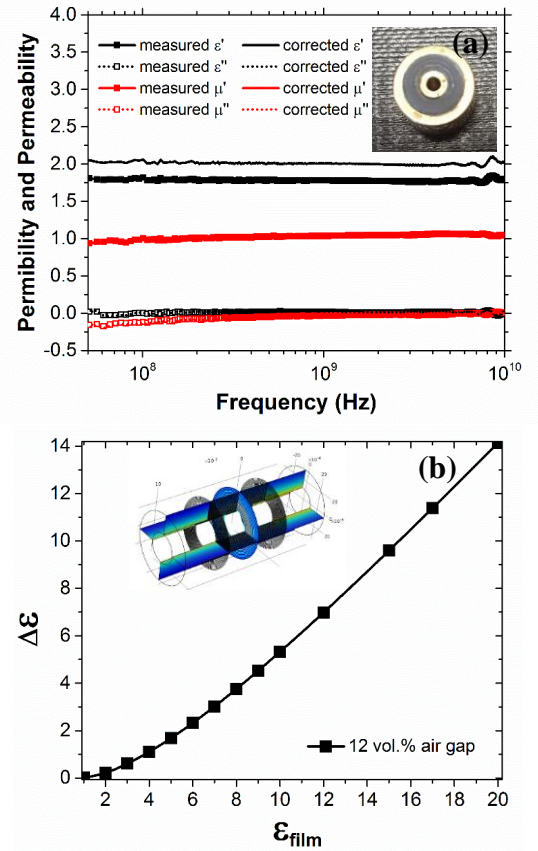


Fig. 2(a) Measured frequency dispersions of the complex permittivity and permeability for a 76 μm PTFE film with 12 vol. % air gap. The inset shows the photograph of the wound PTFE sample inside the coaxial cell. (b) Simulation results of the measured permittivity error ($\Delta\epsilon$) as a function of permittivity for a film with a 12 vol% air gap. The inset shows the electric field magnitude from the Comsol Multiphysics model.

A 3D model of the experimental coaxial line measurement arrangement was established using Comsol Multiphysics RF Module software. Wound films with thickness 76 μm were established in the model along with the air volume fraction of 12 vol. % obtained by experiment, assumed to be distributed equally between each concentric layer. As in experiment, transmission and reflection parameters were retrieved from the model and converted to a real permittivity and real permeability. Fig. 2(b) shows the difference $\Delta\epsilon$ in the simulated permittivity and the actual permittivity of films, as a function of the actual permittivity of the film: the difference increased significantly as the permittivity of the film increased, with an error of almost 50% for a material with a real permittivity of 20. This shows the necessity for applying a correction for the air content if this convenient thin film measurement technique is to be used but, to the best of our knowledge, a suitable approach is not available in the literature.

III. ANALYTICAL MODEL

The background to the correction model is based on a layered capacitor model by Baker-Jarvis [28], which is used to mitigate the uncertainties caused by the air gaps when a bulk toroidal or ring sample is measured in a coaxial cell but where there will generally be an air gap between the sample and the inner conductor, and between the sample and outer conductor. We now extend this approach model to the more complex case of wound thin films, which we simplify as a number of concentric rings, each separated by a small air gap of constant thickness, as shown in Fig. 3.

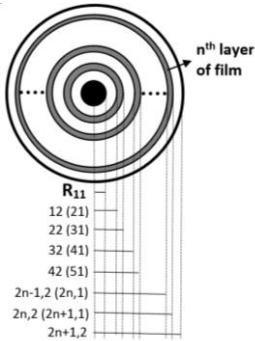


Fig. 3. A schematic representation of a wound film with film layers depicted as series of concentric rings, each separated by an air gap of constant thickness. The radius dimension is defined as $R_{n,j}$, where n denotes the sequence number of layer (either air or film), with $n=1$ is the first inner air layer. $j=1$ denotes the radius considered from center to the inner boundary of n^{th} layer, and $j=2$ is the radius to the outer boundary of n^{th} layer.

With reference to the schematic arrangement in Fig. 3, for the calculation of the gap correction for permittivity, the arrangement can be considered as alternating layers of air and material each acting as a capacitor in series [29], [30].

For capacitors connecting in series:

$$\frac{1}{C} = \frac{1}{C_1} + \frac{1}{C_2} + \dots + \frac{1}{C_n} \quad (1)$$

So that,

$$\frac{1}{C_{\text{mea}}} = \left(\frac{1}{C_1} + \frac{1}{C_3} + \dots + \frac{1}{C_{2n-1}} \right)_{\text{air}} + \left(\frac{1}{C_2} + \frac{1}{C_4} + \dots + \frac{1}{C_{2n}} \right)_{\text{mat}} \quad (2)$$

Where C_{2n-1} and C_{2n} ($n=1, 2, \dots$) are capacitances considering one layer of air and one layer of film respectively and C_{mea} is

the measured effective capacitance of the arrangement as a whole.

The capacitance for a cylindrical geometry is:

$$C = \frac{2\pi\epsilon l}{\ln \frac{R_{\text{outer}}}{R_{\text{inner}}}} \quad (3)$$

where R_{inner} and R_{outer} are the radius of inner conducting cylinder and outer conducting cylindrical shell respectively, l is the cylindrical capacitor length, and ϵ is the dielectric constant of the capacitor medium. Substituting (3) into (2) yields:

$$\frac{1}{C_{\text{mea}}} = \frac{1}{2\pi\epsilon_{\text{air}} l} \left(\ln \frac{R_{12}}{R_{11}} + \ln \frac{R_{32}}{R_{31}} + \dots + \ln \frac{R_{2n-1,2}}{R_{2n-1,1}} \right) + \frac{1}{2\pi\epsilon_{\text{mat}} l} \left(\ln \frac{R_{22}}{R_{21}} + \ln \frac{R_{42}}{R_{41}} + \dots + \ln \frac{R_{2n,2}}{R_{2n,1}} \right) \quad (4)$$

where ϵ_{air} and ϵ_{mat} are the permittivities of air and material respectively. The radius dimension is defined as $R_{n,j}$, where n denotes the layer as either air or film, with $n=1$ at the inner conductor. $j=1$ denotes the radius considered from center to the inner boundary of n^{th} layer, and $j=2$ is the radius to the outer boundary of n^{th} layer.

Equation (4) can be rearranged to:

$$\epsilon_{\text{mat}} = \frac{B}{\left(\ln \frac{R_{2n+1,2}}{R_{11}} \right) / \epsilon_{\text{mea}} - A} \quad (5)$$

where $\epsilon_{\text{mat}} = \epsilon'_{\text{mat}} - j\epsilon''_{\text{mat}}$ is the material actual complex relative permittivity with air gap corrected, $\epsilon_{\text{mea}} = \epsilon'_{\text{mea}} - j\epsilon''_{\text{mea}}$ is the measured uncorrected complex relative permittivity that includes the effect of the air gaps, and:

$$A = \sum_{i=1}^{n+1} \ln \left(1 + \frac{d_{\text{air}}}{R_{2i-1,1}} \right) \quad (6)$$

$$B = \sum_{i=1}^n \ln \left(1 + \frac{d_{\text{mat}}}{R_{2i,1}} \right) \quad (7)$$

R_{11} and $R_{2n+1,2}$ are inner and outer dimensions of the coaxial line, which are 3 mm and 7 mm respectively; d_{air} and d_{mat} are the layer thicknesses of the air layer and film layer respectively.

Similarly, for an air gap correction for the permeability, a series of inductors for the E-field gap is considered:

$$L_{\text{mea}} = (L_1 + L_2 + \dots + L_{2n-1})_{\text{air}} + (L_2 + L_4 + \dots + L_{2n})_{\text{mat}} \quad (8)$$

where L_{2n-1} and L_{2n} ($n=1, 2, \dots$) are inductance considering one layer of air and one layer of film respectively and L_{mea} is the measured effective inductance of the arrangement as a whole, yielding

$$L = \frac{1}{2\pi} \mu \ln \frac{R_{\text{outer}}}{R_{\text{inner}}} \quad (9)$$

where μ is the dielectric constant of the inductor medium.

Substituting (9) into (8) gives:

$$L_{mea} = \frac{\mu_{air}}{2\pi} \left(\ln \frac{R_{12}}{R_{11}} + \ln \frac{R_{32}}{R_{31}} + \dots + \ln \frac{R_{2n-1,2}}{R_{2n-1,1}} \right) + \frac{\mu_{mat}}{2\pi} \left(\ln \frac{R_{22}}{R_{21}} + \ln \frac{R_{42}}{R_{41}} + \dots + \ln \frac{R_{2n,2}}{R_{2n,1}} \right) \quad (10)$$

that can be rearranged to:

$$\mu_{mat} = \frac{\left(\ln \frac{R_{2n+1,2}}{R_{11}} \right) \mu_{mea} - A}{B} \quad (11)$$

where $\mu_{mat} = \mu'_{mat} - j\mu''_{mat}$ is the material actual complex relative permeability with the air gap corrected, $\mu_{mea} = \mu'_{mea} - j\mu''_{mea}$ is the measured uncorrected complex relative permeability that includes the effect of air gaps, and A and B are defined in (6) and (7).

IV. RESULTS AND DISCUSSION

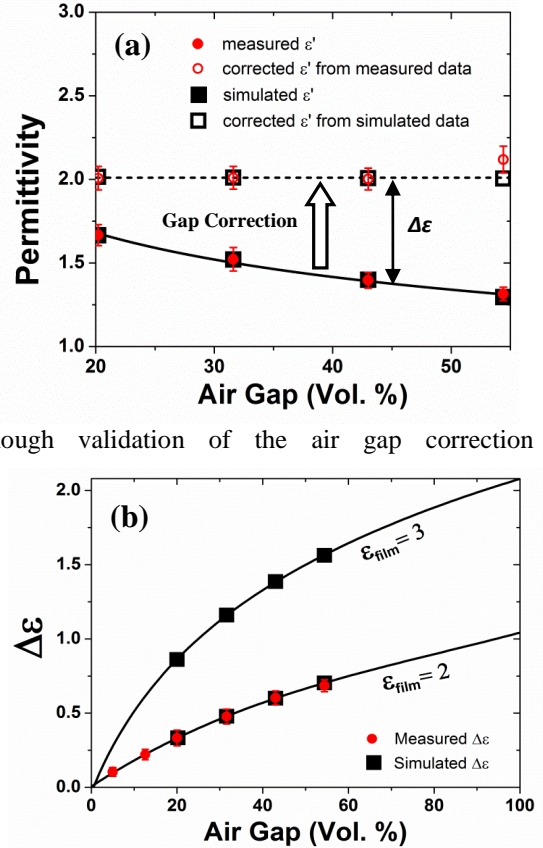
The validity of the air gap correction approach for thin film measurement was assessed by application to measurements of previously well-characterized PTFE films with $\epsilon = 2$. As well as the analytical air gap approach based Equations (1) to (11) above, simulations using the Comsol Multiphysics RF module were also performed with the air gap geometry explicitly represented. Although only isotropic materials are discussed here, the technique is not restricted to measurements on isotropic materials, it can also be used to determine the in-plane anisotropic permeability of a film by rolling the film in different orientations since the magnetic field is in the azimuthal direction. Conversely, due to the electric field being in the radial direction only the permittivity in the direction normal to the film surface can be determined.

The 76 μm thick PTFE films were wound onto a core to form a ring with a range of different tensions in order to produce deliberately different air gap contents. The wound ring length is 7 mm in order to fit into the sample cell. The measured permittivities were approximately constant over the frequency range from 50 MHz up to 10 GHz. Fig. 4(a) shows a comparison between the corrected extracted permittivity as determined from the experiment and the equivalent simulated extracted permittivity for different air gap volume fractions, indicating that the measured permittivities were lower with higher air fractions. The measurement errors mainly came from the random uncertainties that include the noise figure of the VNA used in measuring the magnitude and phase of the scattering parameters, the defects of the coaxial line measurement jig (i.e. impedance match, copper losses of the conductors), the errors in specimen length, specimen positioning, and also the flatness of the wound specimen surface. The system errors caused by the VNA (i.e. coaxial cables, connections, and electronic components) were minimized by a conventional short-open-load-through (SOLT) calibration procedure. The Comsol simulated permittivities were almost exactly coincident with the experimental data. Equation (5) was then applied to the measured permittivities to account for the air gaps and recovered the permittivities in excellent agreement with $\epsilon = 2$ for PTFE at all air fractions below 50%. At 54 vol. % air, the agreement was

reduced because the assumption that the air and film layers were uniformly separated becomes increasingly unrealistic as the air gap fraction increases.

Fig. 4(b) demonstrates the difference $\Delta\epsilon$ in the simulated permittivity and the intrinsic permittivity as a function of air gap volume fraction for two films with an assumed permittivity of 2 and 3. Simulations could not be performed for an air fraction lower than 20 vol. % because of a minimum layer thickness restriction of 17.5 μm in the Comsol software. Fig. 4(b) shows that $\Delta\epsilon$ is larger for films with higher intrinsic permittivity.

To validate the air gap correction method for lossy materials, additional simulations were performed using the complex permittivity of a carbon polymer composite at 8 GHz (15.1-4i) as reported in [31]. The Comsol coaxial line model with a 76 thick film, 20.2 vol. % air gap, and the resulting S-parameters gave a “measured” complex permittivity 3.95-0.20i. This “measured” permittivity was subsequently corrected using Equation (5) resulting in a corrected permittivity of 15.13-3.98i which is coincident with the permittivity of the material.



Although validation of the air gap correction was

Fig. 4 Measured and simulated (a) permittivity of wound PTFE thin films with different air gap volume fractions by experiment and simulation, and permittivity corrected for air gaps using Equation (5); and (b) permittivity adjustment $\Delta\epsilon$ required for a range of air gap volume fractions for films with intrinsic permittivities of 2 and 3.

straightforward for permittivity, the range of available standard films with known complex permeability and frequency dispersion for validation of the permeability correct approach is

very limited. A 100 μm thick sheet of a dispersion of Fe flake powders in an elastomeric matrix (RS Components Ltd) was again wound into a ring on a central axial core and fitted into the co-axial measurement fixture. The measured frequency dispersion of permeability for a measured air gap of 35 vol. % is shown in Fig. 5. Then, following a similar procedure to permittivity, the measured data were introduced into (11) to account for the air gaps to obtain a corrected permeability, which is also shown in Fig. 5. Whilst this corrected permeability lies in the range that might be expected [32], the “true” values of the permeability for the specific film were unknown, leaving simulations as the only way to validate the technique. The corrected values of the permeability from the measurements were used to describe the film properties within the Comsol model and the S-parameters were calculated, from which the permeability *without using any correction for the air gaps* was extracted. If the measurement and correction technique worked correctly, these values would be expected to match the *uncorrected* values from the measurement. These values are also plotted in Fig. 5 and fall exactly on the measured complex permeability curves. Thus, these data shown in Fig. 5 demonstrate that the experimental measurements, their correction for contained gaps using an analytical approach, and the simulations show excellent self-consistency, and when taken with the excellent agreement provided by the same approach for permittivity, suggest a convenient and robust method for permeability correction.

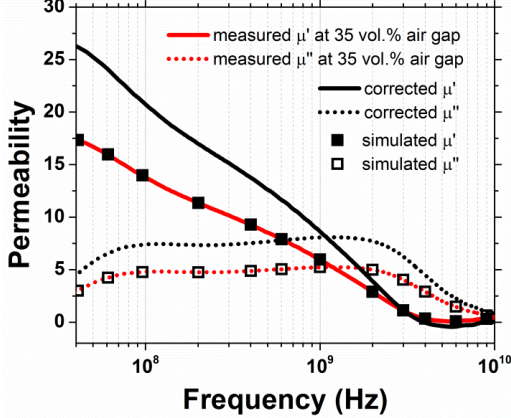


Fig. 5. Frequency dispersions of complex permeability for a wound elastomer + Fe particulate composite 100 μm thick magnetic film with a 35 vol. % air gap. The black solid and dotted lines are the corrected permeability from the measured permeability (red line). Corrected permeability was used in simulations that explicitly included the air gap effect, shown as the open/closed black squares.

To investigate the effect of film thickness in this technique, PTFE films with various thicknesses at different air fractions were studied analytically and by simulation, and values of $\Delta\epsilon$ again obtained, which are shown in Fig. 6 for the various cases. Fig. 6 also shows a polynomial best-fit of $\Delta\epsilon$ for a 76 μm thick PTFE, based on the experiments in Fig. 3(a). Despite changes in the film thicknesses of 25, 35, 50, 100 and 150 μm , the

resulting values of $\Delta\epsilon$ for a constant air fraction lay closely on the best-fit line through the experimental data, demonstrating that film thickness does not have a significant effect on the measured permittivity. In other words, for the same film material, regardless of film thickness, the measured permittivity will be the same for the same overall air volume fraction.

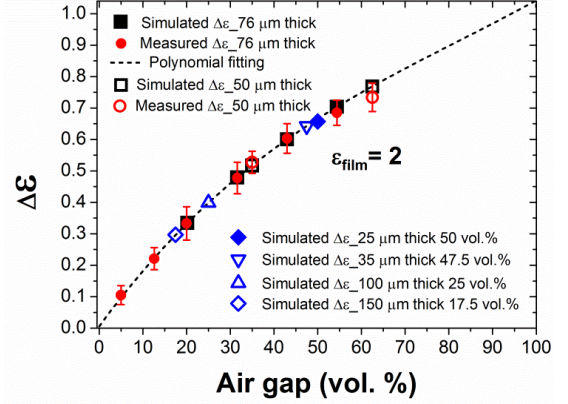


Fig. 6. Permittivity correction as a function of air gap volume fractions for PTFE films of various thicknesses, based on experiment, analysis and simulation.

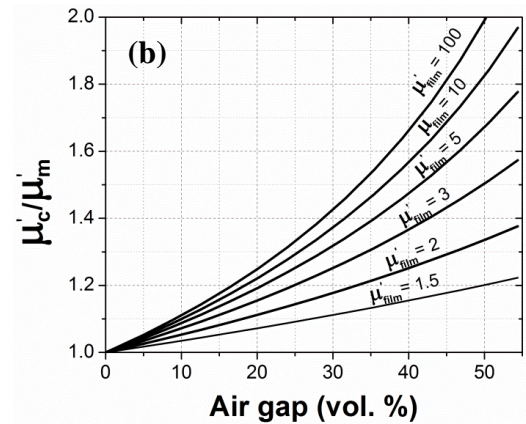
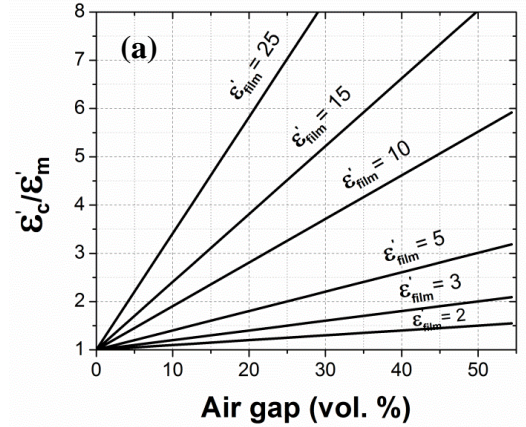


Fig. 7. Air gap correction factor for various values of (a) permittivity and (b) permeability.

Figs. 7(a) and (b) shows the “correction factors” for permittivity and permeability as a function of the air gap volume fraction for different values of intrinsic permittivity and permeability. Here the correction factor is the ratio of the corrected value to the measured uncorrected value i.e. ϵ'_c/ϵ'_m and μ'_c/μ'_m . Figs. 7(a) and (b) can be used as “maps” to estimate a film corrected permittivity and permeability from measured values when the air volume fraction is known. The air gap effect has a more significant effect on permittivity than permeability in the coaxial line arrangement, which is shown in more details in Fig. 8. At the same air gap volume fraction, and for the same measured uncorrected values, the significance of the correction on the extracted permittivity is greater than that on the permeability i.e. at 30 vol. % air gap, $\epsilon'_m = 2$, $\epsilon'_c = 3.4$; $\mu'_m = 2$, $\mu'_c = 2.4$. For permittivity correction, the air gap has a dramatically increasing effect as the air gap fraction is getting large, especially for the measurement of high permittivity materials. In the co-axial arrangement, the azimuthal magnetic field is parallel to the plane of the discontinuity of the air gap between concentric windings of the film and therefore the air gap effect is relatively small. In contrast, the radial electric field is normal to the air gap, resulting in a strong undermining of the measured permittivity and larger correction factor.

The air gap correction for thin film permittivity and permeability measurement using a coaxial line method discussed in this paper could be further extended, for example to films that are supported on a flexible substrate such as Mylar. In this case the three medium system (substrate, coated film, air) could be characterized by a similar extended equivalent circuit. Alternatively, for measurements made as a function of temperature, the air gap fraction may change with temperature because of the different thermal properties of air and film, which again could be accounted for readily in the analysis.

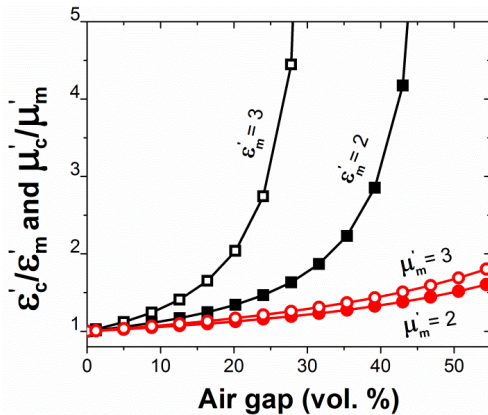


Fig. 8. Air gap correction factor for permittivity and permeability as a function of air gap volume fraction.

V. CONCLUSIONS

A simple broadband (50 MHz – 18 GHz) permittivity and permeability measurement technique for thin films has been developed based on an analytical air gap correction approach for wound samples in a co-axial arrangement. The technique

has been validated for permittivity for well-characterized PTFE films, and by comparison with finite element simulations, over a broad frequency range. The effect of film thickness and air gap volume fraction on the measured permittivity and permeability have been investigated and discussed. This technique may be extended to account for temperature dependent properties of wound films, and for characterization of materials deposited on flexible substrates.

ACKNOWLEDGEMENT

The authors would like to thank the UK Engineering and Physical Sciences Research Council for funding through the programme grant (EP/I034548/1) “The Quest for Ultimate Electromagnetics using Spatial Transforms (QUEST)” and the UK Defence Science and Technology Laboratory for additional financial support. The authors would also like to acknowledge Dr. Baojun Tang for helpful discussion on theoretical model derivation, and Electromagnetic and Acoustic Materials group at University of Exeter for access to equipment.

REFERENCES

- [1] M.J. Lancaster, J. Powell, and A. Porch, “Thin-film Ferroelectric Microwave Devices,” *Supercond. Sci. Technol.*, vol. 11, no. 11, pp. 1323-1334, Nov. 1998.
- [2] N. Gupta, A. Verma, S.C. Kashyap, and D.C. Dube, “Microstructural, Dielectric and Magnetic Behavior of Spin-deposited Nanocrystalline Nickel-zinc Ferrite Thin Film for Microwave Applications,” *J. Magn. Magn. Mater.*, vol. 308, no. 1, pp. 137-142, Jan. 2007.
- [3] E. Hakansson, A. Amiet, S. Nahavandi, and A. Kaynak, “Electromagnetic Interference Shielding and Radiation Absorption in Thin Polypyrrole Films,” *Eur. Polym. J.*, vol. 43, no. 1, pp. 205-213, Jan. 2007.
- [4] S.M. Abbas, M. Chandra, A. Verma, R. Chatterjee, and T.C. Goel, “Complex Permittivity and Microwave Absorption Properties of a Composite Dielectric Absorber,” *Composites: Part A*, vol. 37, no. 11, pp. 2148-2154, Nov. 2006.
- [5] S.S. Kim, S.T. Kim, J.M. Ahn, and K.H. Kim, “Magnetic and Microwave Absorbing Properties of Co-Fe Thin Films Plated on Hollow Ceramic Microspheres of Low Density,” *J. Magn. Magn. Mater.*, vol. 271, no. 1, pp. 39-45, Apr. 2004.
- [6] A. Shalabney and I. Abdulhalim, “Electromagnetic Fields Distribution in Multilayer Thin Film Structures and the Origin of Sensitivity Enhancement in Surface Plasmon Resonance Sensors,” *Sens. Actuators, A*, vol. 159, no. 1, pp. 24-32, Apr. 2010.
- [7] Y. Yang, L. Ma, and J. Wu, “Organic Thin-Film Memory,” *MRS Bull.*, vol. 29, no. 11, pp. 833-837, Nov. 2004.
- [8] D.A. Thompson, L.T. Romankiw, and A.F. Mayadas, “Thin Film Magnetoresistors in Memory, Storage, and Related Applications,” *IEEE Trans. Magn.*, vol. 11, no. 4, pp. 1039-1050, Jul. 1975.
- [9] C.A. Grimes and J.V. Prodan, “Swept Frequency Permeameters for Measuring the Complex, Off-diagonal Permeability Tensor Components of Anisotropic, Thin Magnetic Films,” *J. Appl. Phys.*, vol. 73, no. 10, pp. 6889-6991, May 1993.
- [10] H. Koyama, H. Tsujimoto, and R. Shirai, “Permeability of CoNbZr Amorphous Thin Films Over a Wide Frequency Range,” *IEEE Trans. J. Magn. in Japan*, vol. 2, no. 9, pp. 815-820, Sep. 1987.
- [11] R.C. Taber, “A Parallel Plate Resonator Technique for Microwave Loss Measurements on Superconductors,” *Rev. Sci. Instrum.*, vol. 61, no. 8, pp. 2200-2206, Apr. 1990.
- [12] J. Baker-Jarvis, M.D. Janezic, B.F. Riddle, R.T. Johnk, P. Kabos, C.L. Holloway, R.G. Geyer, and C.A. Grosvenor, “Measuring the Permittivity and Permeability of Lossy Materials: Solids, Liquids, Metals, Building Materials, and Negative-Index Materials” *NIST Tech. Note*, National Institute of Standards and Technology, Boulder, CO., vol. 1536, Feb. 2005.
- [13] Y. Yeow, Z. Abbas, and K. Khalid, “Application of Microwave Moisture Sensor for Determination of Oil Palm Fruit Ripeness,” *Meas. Sci. Rev.*, vol. 10, no. 1, pp. 7-14, Feb. 2010.

- [14] R. Luebbers, "Effect of Waveguide Wall Grooves used to Hold Samples for Measurement of Permittivity and Permeability," *IEEE Trans. Microw. Theory Techn.*, vol. 41, no. 11, pp. 1959-1964, Nov. 1993.
- [15] R. Marks and D. Williams, "A General Waveguide Circuit Theory," *J. Res. Natl. Bur. Stand.*, vol. 97, no. 5, pp. 533-535, Sep. 1992.
- [16] M.D. Janezic, D.F. Williams, V. Blaschke, A. Karamcheti, and C.S. Chang, "Permittivity Characterization of Low-k Thin Films From Transmission-Line Measurements," *IEEE Trans. Microw. Theory Techn.*, vol. 51, no. 1, pp. 132-136, Jan. 2003.
- [17] M.D. Janezic and D.F. Williams, "Permittivity Characterization from Transmission-line Measurement," *IEEE MTT-S Int. Microwave Symp. Dig.*, vol. TH2D-5, pp. 1343-1346, Jun. 1997.
- [18] Y. Liu, L. Chen, C.Y. Tan, H.J. Liu, and C.K. Ong, "Broadband Complex Permeability Characterization of Magnetic Thin Films using Shorted Microstrip Transmission-line Perturbation," *Rev. Sci. Instrum.*, vol. 76, no. 6, pp. 063911, Jun. 2005.
- [19] V. Bekker, K. Seemann, and H. Leiste, "A New Strip Line Broad-band Measurement Evaluation for Determining the Complex Permeability of Thin Ferromagnetic Films," *J. Magn. Magn. Mater.*, vol. 270, no. 3, pp. 327-332, Apr. 2004.
- [20] J. Jiang, G. Du, Y. Yao, C. Liu, L. Yuan, S. Bie, X. Zhang, and H. He, "A New Perturbation Method for Determining the Broadband Complex Permeability of Magnetic Thin Films," *J. Magn. Magn. Mater.*, vol. 320, no. 5, pp. 750-753, Mar. 2008.
- [21] M. Ledieu, F. Schoenstein, J.-H. Le Gallou, O. Valls, S. Queste, F. Duverger, and O. Acher, "Microwave Permeability Spectra of Ferromagnetic Thin Films over a Wide Range of Temperatures," *J. Appl. Phys.*, vol. 93, no. 10, pp. 7202-7204, May 2003.
- [22] S.N. Starostenko, K.N. Rozanov, and A.V. Osipov, "A Broadband Method to Measure Magnetic Spectra of Thin Films," *J. Appl. Phys.*, vol. 103, no. 7, pp. 07E914, Oct. 2008.
- [23] A.M. Nicolson and G.F. Ross, "Measurement of the Intrinsic Properties of Materials by Time-Domain Techniques," *IEEE Trans. Instrum. Meas.*, vol. 19, no. 4, pp. 377-382, Nov. 1970.
- [24] W.B. Weir, "Automatic Measurement of Complex Dielectric Constant and Permeability at Microwave Frequencies," *Proc. IEEE*, vol. 62, no. 1 pp. 33-36, Jan. 1974.
- [25] A.-L. Adenot, O. Acher, D. Pain, F. Duverger, M.-J. Malliavin, D. Damiani, and T. Taffary, "Broadband Permeability Measurement of Ferromagnetic Thin Films or Microwires by a Coaxial Line Perturbation Method," *J. Appl. Phys.*, vol. 87, no. 9, pp. 5965-5967, May 2000.
- [26] O. Acher, J.L. Vermeulen, P.M. Jacquart, J.M. Fontaine, and P. Baclet, "Permeability Measurement on Ferromagnetic Thin Films from 50 MHz up to 18 GHz," *J. Magn. Magn. Mater.*, vol. 136, no. 3, pp. 269-278, Sep. 1994.
- [27] P.G. Lederer, "A Transmission Line Method for the Measurement of Microwave Permittivity and Permeability," *Royal Signals & RADAR Establishment Memorandum*, vol. 4450, Dec. 1990.
- [28] J. Baker-Jarvis, M.D. Janezic, J.H.J. Grosvenor, and R.G. Geyer, "Transmission/Reflection and Short-Circuit Line Methods for Measuring Permittivity and Permeability," *NIST Tech. Note*, National Institute of Standards and Technology, Boulder, CO., vol. 1355, pp. 49-50, Dec. 1993.
- [29] W.P. Westpal, "Techniques of Measuring the Permittivity and Permeability of Liquids and Solids in the Frequency Range 3 c/s to 50 kMc/s," *Lab. for Insulation Research Tech. Report*, MIT, 1950.
- [30] R.L. Jesch, "Dielectric Measurements of Five Different Soil Textural Types as Functions of Frequency and Moisture Content," *Nat. Bur. Stand. (U.S.) Tech. Rep. Report NBSIR 78-896*, Dec. 1978.
- [31] I.M. De Rosa, F. Sarasini, M.S. Sarto, and A. Tamburrano, "EMC Impact of Advanced Carbon Fiber/Carbon Nanotube Reinforced Composites for Next-Generation Aerospace Applications," *IEEE Trans. Electromagn. Compat.*, vol. 50, no. 3, pp. 556-563, Aug. 2008.
- [32] F.S. Wen, L. Qiao, H.B. Yi, D. Zhou, and F.S. Li, "Calculation of High Frequency Complex Permeability of Carbonyl Iron Flakes in a Nonmagnetic Matrix," *Chin. Phys. Lett.*, vol. 25, no. 2, pp. 751-754, Feb. 2008.